LPE Growth of Crack-Free PbSe Layers on Si(100) Using MBE-Grown $PbSe/BaF_2/CaF_2$ Buffer Layers

B.N. STRECKER, P.J. McCANN, and X.M. FANG

School of Electrical and Computer Engineering and Laboratory for Electronic Properties of Materials, University of Oklahoma, Norman, OK 73019

R.J. HAUENSTEIN and M. O'STEEN

Department of Physics, Oklahoma State University, Stillwater, OK 74078

M.B. JOHNSON

Department of Physics and Astronomy and Laboratory for Electronic Properties of Materials, University of Oklahoma, Norman, OK 73019

Crack-free PbSe on (100)-oriented Si has been obtained by a combination of liquid phase epitaxy (LPE) and molecular beam epitaxy (MBE) techniques. MBE is employed first to grow a $PbSe/BaF_2/CaF_2$ buffer structure on the (100)-oriented Si. A 2.5 μm thick PbSe layer is then grown by LPE. The LPE-grown PbSe displays excellent surface morphology and is continuous over the entire 8×8 mm^2 area of growth. This result is surprising because of the large mismatch in thermal expansion coefficients between PbSe and Si. Previous attempts to grow crack-free PbSe by MBE alone using similar buffer structures on (100)-oriented Si have been unsuccessful. It is speculated that the large concentration of Se vacancies in the LPE-grown PbSe layer may allow dislocation climb along higher order slip planes, providing strain relaxation.

Key words: IV-VI semiconductors, BaF_2, CaF_2, PbSe

INTRODUCTION

The temperature tunability and narrow spectral width of lead chalcogenide (IV-VI) tunable diode lasers (TDLs) allow monitoring of many gases.[1,2] Because of these capabilities, TDLs are used for pollution monitoring, process monitoring, and medical diagnostics.[2] However, cryogenic cooling requirements and device cost prevent their wider application. Many groups have fabricated IV-VI lasers using molecular beam epitaxy (MBE)[3–6] and liquid phase epitaxy (LPE)[7–13] grown structures. Such lasers are also commercially available from Laser Photonics in Andover, Massachusetts and Laser Components, GmbH in Olching, Germany. These commercial lasers consist of structures grown on IV-VI substrates which are unavailable in large dimensions and are thermally resistive. (Thermal conductivities of PbSe and PbTe are 0.018 W/cmK[14] and 0.020 W/cmK,[14] respectively.) These values compare poorly with Cu (4.01 W/cmK).[15] The ability to grow high quality, crack-free PbSe on Si(100) will provide larger, lower-cost substrates and is an important step toward the fabrication of thermoelectrically cooled devices.[16]

The (100) orientation of Si provides certain advantages over either (111) or (110). First, Si(100) based technology is more developed; the silicon processing industry prefers this orientation due to its lower density of traps at the Si/SiO_2 interface.[17] Second, device fabrication requirements of IV-VI based lasers favor growth on (100)-oriented substrates. PbSe cleaves preferentially along its {100} planes,[18] producing faces parallel and perpendicular to each other and perpendicular to the epilayer surface; for PbSe grown on Si(111), the {100} planes are angled with respect to the epilayer surface, preventing Fabry-Perot cavity formation.

Island growth, misorientation, and thermal stress induced cracking have hampered growth of continuous epilayers of IV-VI materials on Si(100). Although MBE growth procedures overcoming the problems of island growth and misorientation in the BaF_2/CaF_2 buffer layers have been developed,[19] there have been no reports of crack-free PbSe growth on this surface.

(Received November 25, 1996; accepted January 29, 1997)

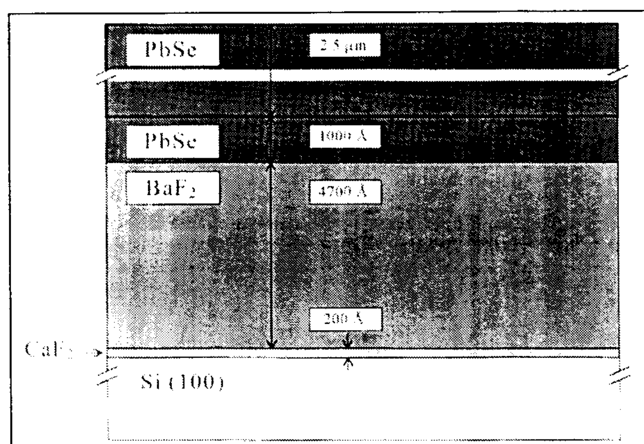

Fig. 1. Schematic of a crack-free PbSe on Si(100) structure. MBE-grown BaF_2 and CaF_2 overcome the lattice mismatch between the Si substrate and PbSe layers. 1000Å of MBE-grown PbSe permit low temperature LPE growth of the uppermost 2.5 µm of PbSe.

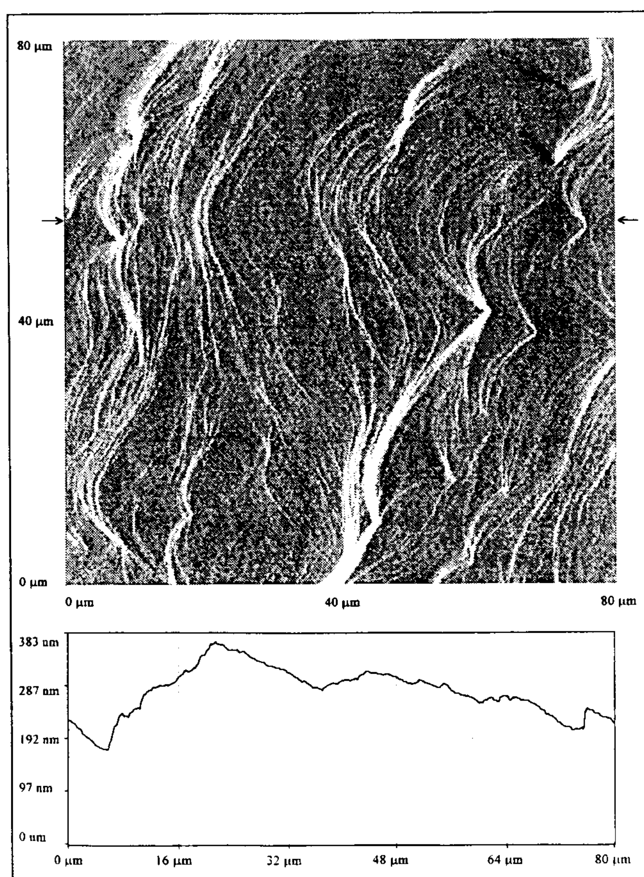

Fig. 2. Contact-mode AFM scan of sample W113-1, an LPE-grown PbSe layer on Si(100) exposed to a minimum temperature of 300K. To accentuate sample relief, the scan is displayed in a shadowing mode, simulating a light source on the left. A line scan, indicated by the arrows, shows a peak-to-peak roughness of about 200 nm and presents the true surface topography. The 80 × 80 µm² surface is free of cracks, inclusions, and melt adhesion.

This article discusses experiments which demonstrate that addition of an LPE-grown PbSe layer on MBE-grown PbSe/BaF_2/CaF_2 suppresses thermally induced cracking and produces continuous (100)-oriented PbSe layers on Si(100).

EXPERIMENT

Epitaxial growth of PbSe on Si (100) proceeded in two phases: MBE growth of a thin PbSe layer on Si(100) using BaF_2 and CaF_2 buffer layers followed by LPE growth of a thick PbSe layer on the MBE-grown structure.

Molecular Beam Epitaxy Growth

Growth was performed on p-type Si(100) in an Intevac Gen II MBE system. Wafers were cleaned by the Shiraki method[20] prior to loading and heated to 1000°C for 30 min in the growth chamber to remove the Shiraki-grown oxide. After oxide desorption, a 200Å CaF_2 layer was grown while the wafer temperature was held at 580°C. This was followed by a 3200Å layer of BaF_2 (substrate temperature 580°C), annealing at 800°C for 3 min,[19] and growth of an additional 1500Å of BaF_2 (substrate temperature 700°C). The final MBE layer was 1000Å of PbSe (substrate temperature 260°C) grown from a single PbSe effusion cell.

Liquid Phase Epitaxy Growth

The Si(100) wafer, with the MBE-grown layers, was cleaved into 1 × 1 cm squares, which were then used as substrates for subsequent LPE growth with no further preparation. Melt constituents, Pb and PbSe, were placed in a graphite boat and heated to 650°C in a hydrogen atmosphere for approximately 2 h to homogenize the melt. The furnace and boat used for the LPE growth are described elsewhere.[21,22] Chalcogenide concentration was set to 0.20 wt% based upon previously published phase equilibria data for PbSe.[23] Nucleation and liquidus temperatures for the melt were measured by observing the temperature for the initial formation of nuclei during cooling and dissolution of the last nucleus during warming. The furnace was then cooled to room temperature before being opened to introduce the substrate. Furnace temperature was subsequently kept below 500°C to minimize the thermal stress applied to the MBE-grown epilayers. Growth was initiated by pulling the substrate under the melt at 2°C above the measured nucleation temperature (near 470°C) as the melt was being cooled at 2°C per min. The epilayer grew for 40 min, at which time growth was terminated by pulling the substrate out from under the melt. The furnace was turned off and the system allowed to cool to room temperature before being flushed with argon and opened to atmosphere. The resulting structure is shown schematically in Fig. 1.

RESULTS

Optical Nomarski microscopy, scanning electron microscopy (SEM), contact mode atomic force microscopy (AFM), and high resolution x-ray diffraction (HRXRD) were used to examine the layers. Figure 2 shows a 80 × 80 µm² scan of the surface of sample W113–1, an LPE-grown PbSe layer on (100)-oriented Si which was grown as described above. The image

was obtained with a TopoMetrix Explorer AFM system operating in contact mode and shows the region to be crack-free. The scan indicated a peak-to-peak surface roughness of approximately 0.25 μm for the layer. Figure 3 is a similar scan of the sample after temperature cycling to 77K. It shows (100)-oriented cracks spaced approximately 50 μm apart. An SEM cross-section of sample W113-1 after temperature cycling to 77K, Fig. 4, shows that the crack examined extends through the PbSe layer, perpendicular to its surface. The 2.5 μm layer thickness visible in the SEM micrograph was verified by a Tencor scan profiler.

The SEM micrograph of sample W113-B66 in Fig. 5 was taken at the boundary of the LPE melt contact and shows the surface morphologies of LPE-grown (lower half of photograph) and MBE-grown (upper half of photograph) layers. Since the horizontal well dimensions of the graphite boat are smaller than the substrate width, a portion of the substrate is left exposed, providing a comparison of the materials obtained by the two PbSe growth techniques. While approximately 10^6 cracks/cm^2 are visible in the MBE grown layer, no cracking is visible in the LPE-grown region. Optical Nomarski microscope observation of the uncycled LPE-grown PbSe layer of this sample revealed three (100)-oriented cracks across the sample. It should be noted, however, that sample W113-B66 varied from the growth procedure described above by being inserted into the LPE furnace before homogenizing the melt. The cracking observed in this sample has been attributed to the higher temperature to which it was exposed prior to LPE layer growth. Sample W113-1 was not exposed to the high temperature homogenization step, and no cracks were observed by either both optical Nomarski or AFM examination.

A Philips MRD four-bounce monochromator x-ray diffraction system was also used to investigate crystal

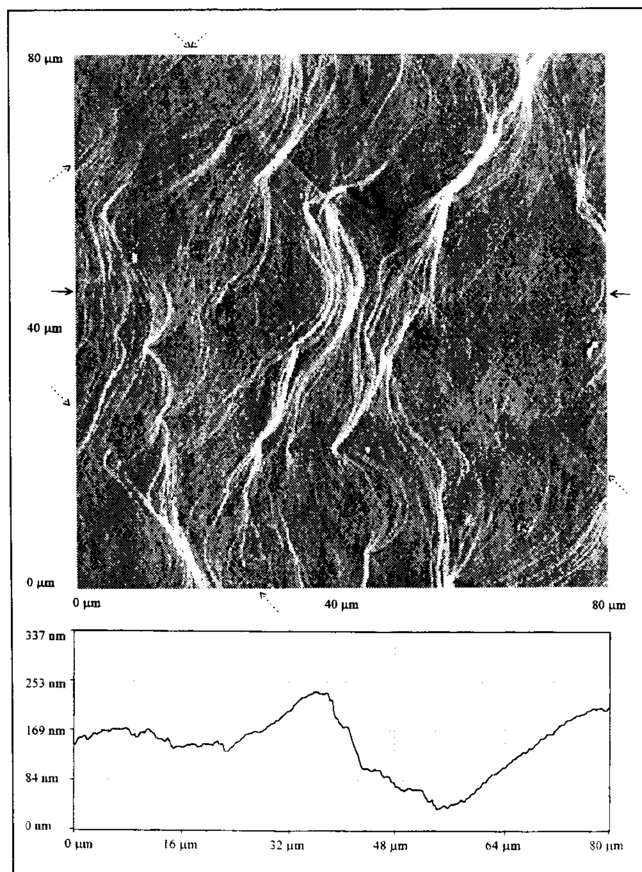

Fig. 3. Contact-mode AFM scan of sample W113-1, an LPE-grown PbSe layer on Si(100), after cooling to 77K and warming to 300K. To accentuate sample relief, the scan is displayed in a shadowing mode, simulating a light source on the left. A line scan, indicated by the solid arrows, shows a peak-to-peak roughness of about 220 nm and presents the true surface topography. Two parallel (100)-oriented cracks, spaced by approximately 50 μm, and a (100)-oriented crack perpendicular to them are indicated by dotted arrows.

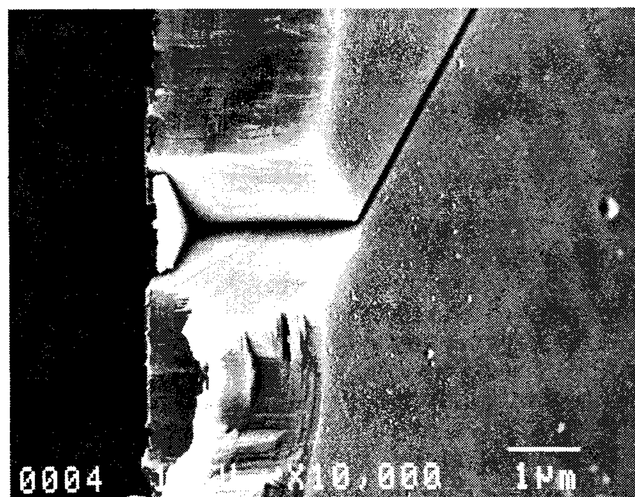

Fig. 4. SEM micrograph of a cross-section of sample W113-1, an LPE-grown PbSe layer on Si(100) cleaved along one of the {110} planes, after cooling to 77K and warming to 300K. LPE-grown PbSe occupies the right side of the micrograph; the thin buffer layer structure is visible separating it from the Si substrate on the left. A crack having parallel (100)-oriented faces extends to the substrate surface.

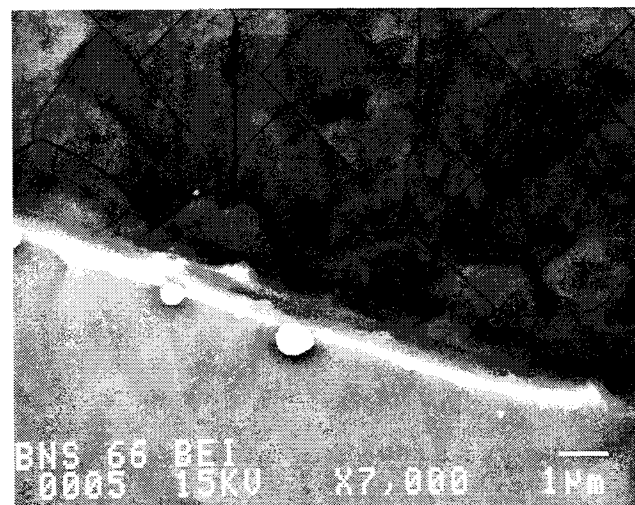

Fig. 5. SEM micrograph of the LPE melt contact boundary of sample W113-B66. The surface of the cracked MBE-grown PbSe layer occupies the upper half of the micrograph. The surface of the uncracked LPE-grown PbSe layer is shown in the lower half. Small spheres of melt adhesion dot the boundary.

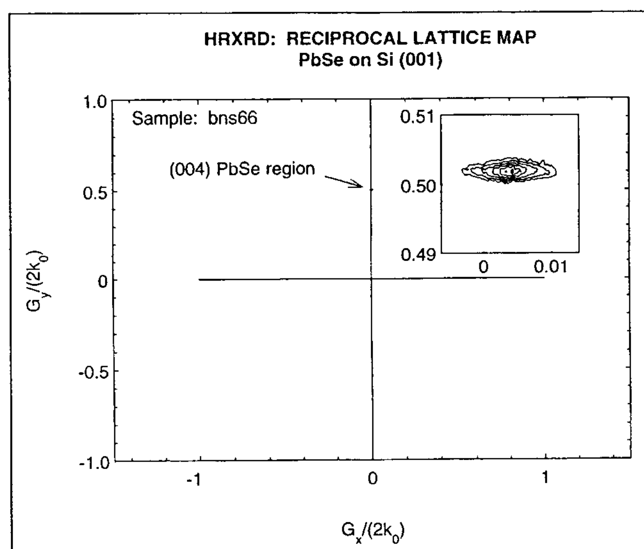

Fig. 6. Reciprocal space plot of the (004) reflection of a PbSe(100) layer grown on Si(100) by LPE. The inset shows the shift of the PbSe (004) reflection to the right of the vertical axis, which has been aligned to the Si(100) substrate.

quality. Both rocking curve and θ-2θ measurements about the symmetric (004) Bragg reflection were performed to separately assess PbSe epitaxial material quality with respect to mosaic tilt spread as well as inhomogeneous strain broadening (d-spacing variation) along the growth direction. Additionally, for selected samples, "reciprocal-space maps" (constant-diffracted-intensity contours in the reciprocal space diffraction plane) of the PbSe (004) peak were recorded. A representative reciprocal-space map is given in Fig. 6. From the figure, it is evident (see inset) that the diffraction peak is of considerably greater extent in reciprocal space along the in-plane directions than along the growth direction. The large in-plane peak width is most commonly attributed to mosaic spread while the growth direction peak broadening is, in general, a measure of both inhomogeneous strain and finite crystal coherence length effects along the growth direction, due to the presence of a high density of misfit-relieving threading dislocations, stacking faults, or other extended defects. In view of the large lattice mismatch (~1% for BaF_2 and PbSe, ~14% for Si and PbSe) between the PbSe layers and the substrate, this is not surprising, and, in fact, has been observed in other highly lattice-mismatched material system such as GaN on Al_2O_3.[24]

To better characterize these separate peak-broadening effects, a set of rocking curve scans, as well as θ-2θ scans (in both cases with a 0.45 mm receiving slit placed in front of the detector), were performed for each sample. The rocking-curve and θ-2θ scans correspond to profiling the PbSe (004) reciprocal-space feature of Fig. 5 along its widest and narrowest aspects, respectively. In all cases, the θ-2θ scans yield narrow, Gaussian peaks with FWHM values ranging from 200–250 arcsec. On the other hand, rocking curve measurements of the same PbSe (004) reflections exhibit comparatively broader peaks with *exponential* tails. This latter observation suggests that the (004) planes of the PbSe layer are approximately exponentially distributed in angle over a small range of tilts (FWHM from ~600–1200 arcsec in our initial samples to as little as ~350 arcsec for W113–1 as epitaxial growth procedures became improved) about some mean value. As can be seen from Fig. 6, the PbSe (004) peak is slightly displaced from the ordinate, indicating that the mean PbSe [004] (hence [001]) direction is *not* aligned parallel to that of the substrate. In fact, we have ascertained through HRXRD examination of the substrate that our nominally (001)-oriented Si substrates are actually slightly vicinal (off axis by ~0.85°), and that the mean PbSe [001] direction appears to be rotated by ~0.35° relative to that of the substrate in a direction toward the actual substrate normal. It is possible that this net rotation of the epitaxial structure occurs as an additional mechanism to (partially) accommodate the rather large epitaxial-substrate lattice mismatch; the origin of the rotation effect is still under investigation.

DISCUSSION

Growth of CaF_2 (lattice parameter 5.46305Å at 300 K)[25] on Si(100) using a two temperature process produces flat (100)-oriented CaF_2 layers in spite of CaF_2's tendency toward (111) faceting due to the lower surface energy of the (111) faces.[26] By following CaF_2 growth with BaF_2 (6.2001Å),[27] PbSe (6.1243Å)[28] can be grown with much smaller lattice mismatch (1.2%) than growth directly on CaF_2. An additional benefit of this structure is that the incorporated BaF_2 layer is water soluble and can be used as a release layer, enabling epitaxial lift-off of structures from the silicon substrate.[16]

The high density of cracks (approximately 10^6 cm^{-2}) in the MBE-grown PbSe is clearly caused by the large mismatch of thermal expansion coefficients between the Si substrate and the CaF_2, BaF_2, and PbSe layers. (The thermal expansion coefficients, given at 300K, are 2.6×10^{-6} K^{-1} for Si and $19.2–19.8 \times 10^{-6}$ K^{-1} for the epilayers.)[29] As the wafer cools from its final MBE growth temperature of 280°C, the PbSe and fluoride buffer layers contract more rapidly than the silicon substrate, large tensile stress is generated in the layers, and cracks form. It is also possible that the MBE-grown PbSe is "cracked" when grown, due to pre-existing cracks in the BaF_2 surface caused by cooling from the BaF_2 growth temperature (700°C) to the PbSe growth temperature (280°C) and a failure of the PbSe to grow down the crack walls or bridge them.

The thermal expansion mismatch between the layers and substrate requires that the LPE growth temperature for the final PbSe layer be as close to room temperature as possible. The MBE-grown PbSe allows this lower temperature LPE growth. Earlier studies of LPE growth of PbSe on BaF_2(100) substrates demonstrated that growth must begin near 625°C,[23] which corresponds to the formation of a BaSe reaction layer[30] that can catalyze PbSe nucleation.[31] Attempts to grow PbSe on BaF_2/CaF_2/Si(100) without

the MBE-grown PbSe layer required such elevated temperatures and resulted in poor layer quality with inclusions, a large number of cracks, and melt adhesion. The limiting factor for low temperature LPE growth of PbSe is the chalcogenide concentration in the melt. Nucleation temperature of the melt decreases to the melting point of Pb (327°C) as the concentration of Se is reduced. However, attempts to grow PbSe from melts with a chalcogenide concentration less than about 0.20 %wt resulted in discontinuous layers, due to Se solute depletion between growing nuclei on the substrate surface. At this concentration, the LPE growth initiation temperature is still 210°C higher than the growth temperature for the MBE-grown PbSe. It is hypothesized that this provides a smooth, compressed surface of MBE-grown PbSe during LPE growth, as long as the temperature is not too high. In which case, the MBE-grown PbSe is damaged by the excessive compression and perhaps buckles.

The primary glide plane system in PbSe is along the (100) planes in the [110] direction.[18] For growth on (100)-oriented substrates, these planes are perpendicular to the surface, have zero valued Schmid factors and are incapable of relieving the thermally induced stress. However, higher order glide planes may exist which have nonzero Schmid factors and are able to relieve the stress. Previous work by Maissen[32] has detected slip lines in (100)-oriented MBE-grown PbSe on Si using STM. It is possible that the high concentration of Se vacancies (10^{18}–10^{19} cm^{-3})[33] in the LPE-grown PbSe provides a mechanism for dislocation climb,[34] which relieves the stress or interacts with dislocations moving along the higher order glide planes, making them more mobile. This is the most likely explanation for our successful growth of crack-free PbSe layers on (100)-oriented Si.

CONCLUSION

High quality (100)-oriented PbSe layers have been grown by LPE on Si(100) using an MBE-grown PbSe/BaF_2/CaF_2 buffer. The MBE-grown PbSe allows for lower temperature LPE growth and reduced stress in the system compared to that required for growth without the PbSe. This results in crack-free (100)-oriented PbSe on Si(100) and a high quality, low cost substrate for subsequent growth of IV-VI laser structures. In addition, the MBE-grown BaF_2 layer incorporated into the buffer allows epitaxial lift off of such IV-VI laser structures. Remounting on a more thermally conductive material, such as copper, has been predicted to provide a large increase in operating temperature over the current generation of lasers grown on IV-VI substrates. This work can thus lead to the fabrication of lasers that operate at temperatures obtainable by thermoelectric coolers.

ACKNOWLEDGMENTS

The authors thank Harpreet Sachar for assistance with LPE growth, Bill Chissoe for assistance with SEM analysis, and the National Science Foundation, grant number DMR-9416871, for financial support.

REFERENCES

1. E.V. Stepanov, A.I. Kouznetsov, P.V. Zyrianov, V.G. Plotnichenko, Yu. G. Selivanov and V.G. Artjushenko, *Infrared Phys. and Technol.* 37, 149 (1996).
2. J.F. Becker, T.B. Sauke and M. Loewenstein, *Appl. Opt.* 31, 1921 (1992).
3. M. Tacke, B. Spanger, A. Lambrecht, P.R. Norton and H. Böttner, *Appl. Phys. Lett.* 53, 2260 (1988).
4. Z. Feit, M. McDonald, R.J. Woods, V. Archambault and P. Mak, *Appl. Phys. Lett.* 68, 738 (1996).
5. J.N. Walpole, A.R. Calawa, T.C. Harman and S.H. Groves, *Appl. Phys. Lett.* 28, 552 (1976).
6. D.L. Partin and W. Lo, *J. Appl. Phys.* 52, 1579 (1981).
7. D. Kasemset and C.G. Fonstad, *Appl. Phys. Lett.* 39, 872 (1981).
8. Y. Horikoshi, M. Kawashima and H. Saito, *Jpn. J. Appl. Phys.* 20, L897, (1981).
9. J.P. Moy and J.-Ph. Reboul, *Infrared Phys.* 22, 163 (1982).
10. S.H. Groves, K.W. Nill and A.J. Strauss, *Appl. Phys. Lett.* 25, 331 (1974).
11. A. Shahar and A. Zussman, *Infrared Phys.* 27, 45 (1987).
12. Y. Nishijima and K. Shinohara, *Appl. Opt.* 32, 4485 (1993).
13. Z. Feit, J. Fuchs, D. Kostyk and W Jalenak, *Infrared Phys. and Technol.* 37, 439 (1996).
14. G.E. Childs, L.J. Ericks and R.L. Powell, *Thermal Conductivity of Solids at Room Temperature and Below* (National Bureau of Standards, 1973).
15. C. Kittell, *Introduction to Solid State Physics,* 6th ed. (New York: John Wiley and Sons, 1986).
16. P.J. McCann and K.R. Lewelling, *Optical Remote Sensing for Environmental and Process Monitoring*, (Pittsburgh, PA: Air and Waste Management Association, 1996), p. 26.
17. S.M. Sze, *Physics of Semiconductor Devices*, 2nd ed. (New York: John Wiley and Sons, 1981).
18. P. Müller, A. Fach, J. John, A.N. Tiwari, H. Zogg and G. Kostorz, *J. Appl. Phys.* 79, 1911 (1996).
19. X.M. Fang, P.J. McCann and W.K. Liu, *Thin Solid Films* 272, 87 (1996).
20. A. Ishizaka and Y. Shiraki, *J. Electrochem. Soc.: Electrochem. Sci. and Technol.* 133, 666 (1986).
21. P.J. McCann, J. Fuchs, Z. Feit and C.G. Fonstad, *J. Appl. Phys.* 62, 2994 (1987).
22. P.J. McCann and S.K. Aanegola, *J. Cryst. Growth* 141, 376 (1994).
23. P.J. McCann and C.G. Fonstad, *J. Cryst. Growth* 114, 687 (1991).
24. D. Kapolnek, X.H. Wu, B. Heying, S. Keller, B.P. Keller, U.K. Mishra, S.P. DenBaars and J. S. Speck, *Appl. Phys. Lett.* 67, 1541 (1995).
25. *Powder Diffraction File* (Swarthmore, PA: Joint Committee on Powder Diffraction Standards, International Center for Diffraction Data, 1986) Card: 35–0816.
26. S. Blunier, H. Zogg and H. Weibel, *Appl. Phys. Lett.* 53, 1512 (1988).
27. H.E. Swanson and E. Tatge, *Standard X-ray Diffraction Powder Patterns*, Circular 539, vol. I (National Bureau of Standards, 1953).
28. H.E. Swanson, N.T. Gilfrich and G.M. Ugrinic, *Standard X-ray Diffraction Powder Patterns,* Circular 539, vol. V (National Bureau of Standards, 1955).
29. H. Zogg, A. Fach, C. Maissen, J. Masek and S. Blunier, *Optical Engineering* 33, 1440 (1994).
30. P.J. McCann and C.G. Fonstad, *J. Electron. Mater.* 20, 915 (1991).
31. P.J. McCann, *Mater. Res. Soc. Symp. Proc.* 221, (Pittsburgh, PA: Mater. Res. Soc., 1991), p. 289.
32. C. Maissen, Ph.D. thesis, Swiss Federal Institute of Technology No. 9930 (1992).
33. P.J. McCann, S.K. Aanegola and J.E. Furneaux, *Appl. Phys. Lett.* 65, 2185 (1994).
34. J.P. Hirth and J. Lothe, *Theory of Dislocations*, 2nd ed., (NY: John Wiley and Sons, 1982).